Control of solid state laser dynamics by semiconductor devices

Franz X. Kärtner
Luigi R. Brovelli
Daniel Kopf
Markus Kamp
Irio Calasso
Ursula Keller
Swiss Federal Institute of Technology
Institute of Quantum Electronics
Ultrafast Laser Physics Laboratory
ETH Hönggerberg—HPT
CH-8093 Zurich, Switzerland
E-mail: kaertner@iqe.phys.ethz.ch

Abstract. We have successfully demonstrated that an appropriately designed semiconductor saturable absorber device, the antiresonant Fabry-Perot saturable absorber, can reliably start and sustain stable mode locking of solid state lasers such as Nd:YAG, Nd:YLF, Nd:Glass, Cr:LiSAF, and Ti:sapphire lasers. Especially for solid state lasers with long upper-state lifetimes, previous attempts to produce self-starting passive mode locking with saturable absorbers was always accompanied by self-*Q*-switching. We derive criteria that characterize the dynamic behavior of solid state lasers in the important regimes of *Q*-switching, mode-locked *Q*-switching, and continuous-wave mode locking in the picosecond and femtosecond range for the pulsewidth. We demonstrate that semiconductor absorbers can be designed to predetermine the dynamic behavior of a laser for a given solid state laser material and present an experimental verification. This allows for the development and design of robust, compact pico- and femtosecond solid state laser sources for scientific and industrial applications.

Subject terms: Q-*switching; passive mode locking; self-starting; solid state lasers.*

Optical Engineering 34(7), 2024–2036 (July 1995).

1 Introduction

There is intensive ongoing research directed toward an all-solid-state ultrafast laser technology. The availability of high-power diode lasers and laser arrays, which can be utilized to pump solid state laser materials very efficiently, allows for more compact, reliable lasers with less utility requirements. New laser materials with extraordinary high intrinsic quantum efficiencies of more than 90% and an improved scalable cavity design make output powers in the kilowatt range from laser heads smaller than a shoe box possible in the near future.[1] Such powerful and compact laser sources will have applications in fundamental research such as x-ray, plasma, and higher-harmonic generation as well as in medicine and industry.

To increase the laser peak power or to obtain ultrashort optical pulses one usually controls the laser dynamics by various *Q*-switching and continuous-wave (cw) mode-locking techniques that have been developed over the last three decades.[2,3] Our research carries the idea of an all-solid-state ultrafast laser technology even further by controlling the laser dynamics with compact scalable passive semiconductor devices. The semiconductor device essentially acts as a saturable absorber. It is well known that a saturable absorber can be used to passively *Q*-switch or mode-lock a laser. But there is a third regime where the laser is *Q*-switched-mode-locked, i.e., mode-locked pulses are underneath the *Q*-switched envelope. For most applications, this is undesirable.

It has been believed for a very long time that solid state lasers such as Nd:YAG or Nd:YLF, with their long upper-state lifetimes, can hardly be passively cw mode locked using saturable absorbers without *Q*-switching or at least *Q*-switched mode locking.[4] However, in this paper we show that, depending on the parameters of the saturable absorber such as the recovery time of the absorption and the saturation energy, pure passive *Q*-switching or pure cw mode locking and, if desired, also *Q*-switched mode locking can be obtained. As a result, full control over the saturable absorber device parameters is required to obtain well-matched optimum values for a given solid state laser material. Bandgap engineering and modern semiconductor growth technology in principle allow for the production of saturable absorbers with accurate control of the device parameters such as bandgap, saturation energy, and carrier lifetime. Semiconductor absorbers have an intrinsic bitemporal pulse response, the scales being given by intraband carrier-carrier scattering and thermalization processes, which are on the order of 10 to

Paper SWI-50 received Nov. 15, 1994; revised manuscript received Jan. 23, 1995; accepted for publication Feb. 13, 1995.

several hundred femtoseconds, and by interband recombination processes, which can be on the order of picoseconds to nanoseconds. This makes such absorbers ideal for the mode locking of solid state lasers in the femtosecond and picosecond regime.

In the first part of this paper we systematically develop basic laser models that describe the dynamics of solid state lasers. Based on these models, we study the most important features of the laser dynamics analytically and derive criteria that characterize the laser dynamics with respect to Q-switching, mode-locked Q-switching, and self-starting of mode locking by a saturable absorber. We show that there is a parameter regime for the absorber where even a solid state laser like Nd:YLF, with its long upper-state lifetime of 450 μs, can be safely cw mode locked without Q-switching. Saturable absorbers with relaxation times in the picosecond range can then generate stable picosecond pulses if the gain bandwidth is broad enough. Furthermore, we demonstrate that with a picosecond absorber one can even generate femtosecond pulses if solitonlike pulse shaping is additionally employed. This is a new regime of mode locking, which we call soliton mode locking by a slow saturable absorber. It is extremely useful for diode-pumped lasers, where Kerr-lens mode locking (KLM) is weak due to the large pump area in the laser crystal. This mode-locking technique also does not impose any requirements on the cavity design or operation of the cavity close to its stability limit. Therefore, soliton mode locking is a stable phenomenon, which allows for a scalable resonator design.

By taking advantage of existing molecular beam epitaxy (MBE) technology, semiconductor elements with the required dynamical behavior can be fabricated. Normally some parameters of the semiconductor material are not well matched to the characteristics required for solid state lasers, because the semiconductors tend to have too much optical loss, too low a saturation intensity, and too low a damage threshold for typical solid-state lasers. One way to solve these problems is the recently developed antiresonant Fabry-Perot saturable absorber (A-FPSA),[5,6] which integrates the semiconductor saturable absorber inside a Fabry-Perot cavity operated at antiresonance with a free spectral range larger than the gain bandwidth of the solid state laser.

The theoretical investigations in Secs. 2 and 3 treat the absorber within a simple two-level rate-equation model. In Sec. 4 we describe the semiconductor absorbers we use. For a large variety of dynamical effects occurring in a laser it is sufficient to model the semiconductor absorber as an equivalent two-level system. We show how we can determine and modify the key parameters of the equivalent two-level model. In Sec. 5, finally, we compare the theory with experiments and demonstrate by the example of a 45-fs diode-pumped Cr:LiSAF laser the usefulness of the described techniques. This paper is not intended to be a complete review of our work, but it gives a firm theoretical foundation for the experimental results obtained so far. This is the basis for an improved absorber design to control the dynamics of solid state lasers.

2 Q-Switching versus Q-switched Mode Locking and CW Mode Locking in Solid State Lasers

In this section we briefly review the results derived by Haus on the parameter ranges for cw Q-switching and cw mode

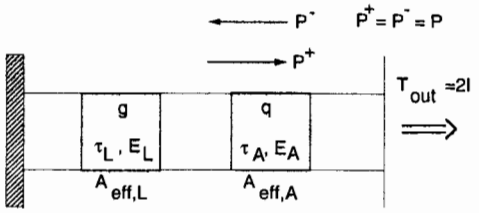

Fig. 1 Simple laser model corresponding to the rate equations (1) to (3). We assume small output coupling T_{out} so that the laser power within one roundtrip does not change very much. Neglecting standing-wave effects in the cavity, the field density is related to twice the circulating power P^+ or P^-.

locking[4] to clarify the notation used and to extend these results to the case of Q-switched mode locking. We start from the simplest laser model of a single-mode laser with homogeneously broadened laser medium and saturable absorber as shown in Fig. 1. We make the following assumptions. First, the transverse relaxation times of the equivalent two-level models for the laser gain medium and for the saturable absorber are much faster than any other dynamics in our system, so that we can use rate equations to describe the laser dynamics.[7] Second, we assume that the changes in the laser intensity, gain, and saturable absorption on a time scale of the order of the round-trip time T_R in the cavity are small (i.e., less than 20%). Then we can write the rate equations of the laser as

$$T_R \frac{dP}{dt} = 2(g - l - q)P \ , \tag{1}$$

$$T_R \frac{dg}{dt} = -\frac{g - g_0}{T_L} - \frac{gT_R P}{E_L} \ , \tag{2}$$

$$T_R \frac{dq}{dt} = -\frac{q - q_0}{T_A} - \frac{qT_R P}{E_A} \ , \tag{3}$$

where P denotes the laser power, g the gain per round trip, l the linear losses per round trip, q the saturable losses per round trip, g_0 the small-signal gain per round trip, and q_0 the unsaturated but saturable losses per round trip. The quantities $T_L = \tau_L / T_R$ and $T_A = \tau_A / T_R$ are the upper-state lifetime of the gain medium and the absorber recovery time, normalized to the round-trip time of the cavity. The energies $E_L = h\nu A_{\text{eff},L} / 2\sigma_L$ and $E_A = h\nu A_{\text{eff},A} / 2\sigma_A$ are the saturation energies of the gain and the absorber, respectively. The factor of 2 in the definition of the saturation energies is due to averaging over the standing-wave effects in a linear cavity. If we use a ring cavity, or if the laser is in pulsed operation and the media are much shorter than the equivalent pulselength, we have to replace 2 with 1. For simplicity we also do not take into account effects due to spatial hole burning, which nevertheless can become important from a quantitative point of view, but will not change the overall qualitative picture.[8] The factor of 2 in Eq. (1) is due to counting gain and loss with respect to amplitude and not with respect to power, for reasons that will become obvious later on.

For solid state lasers with relaxation times of the gain on the order of $\tau_L \approx 100$ μs or more and cavity round-trip times

of $T_R \approx 10$ ns, we obtain $T_L \approx 10^4$. On the other side, we assume absorbers with recovery times much shorter than the round-trip time of the cavity, i.e., $\tau_A \approx 1$ to 100 ps, so that typically $T_A \approx 10^{-4}$ to 10^{-2}. This is achievable in semiconductors and can be engineered at will by low-temperature growth of the semiconductor material.[9,10] Thus as long as the laser is running cw and single mode, the absorber will follow the instantaneous laser power, and we can eliminate the saturable absorption q adiabatically[11] by using Eq. (3). Then we substitute in Eq. (1)

$$q = \frac{q_0}{1 + P/P_A} \quad \text{with} \quad P_A = \frac{E_A}{\tau_A} , \tag{4}$$

where P_A is the saturation power of the absorber. At a certain value of the saturable absorption, the relaxation oscillations become unstable and Q-switching occurs.

2.1 *Parameter Ranges for CW Q-Switching*

A linearized stability analysis of Eqs. (1) and (2) with Eq. (4) gives the stability criterion against Q-switching of the cw-running laser[4]:

$$-2P \frac{\mathrm{d}q}{\mathrm{d}P}\bigg|_{\mathrm{cw}} < \frac{r}{T_L}\bigg|_{\mathrm{cw}} \quad \text{with} \quad r = 1 + \frac{P}{P_L} \text{ and } P_L = \frac{E_L}{\tau_L} , \tag{5}$$

where r is the pump parameter that describes at how many times the threshold the laser operates, and P_L is the saturation power of the laser gain. The inequality (5) has a simple physical explanation. The right side of (5) is the relaxation time to equilibrium for the gain at a given pump power and constant laser power. The left side is the decay time of a power fluctuation of the laser at fixed gain. If the gain cannot react fast enough to fluctuations of the laser power, relaxation oscillations grow and result in passive Q-switching of the laser.

As can be seen from Eqs. (4) and (5), we obtain

$$-2T_L P \frac{\mathrm{d}q}{\mathrm{d}P}\bigg|_{\mathrm{cw}} = 2T_L q_0 \frac{P/\chi P_L}{(1 + P/\chi P_L)^2} < r|_{\mathrm{cw}} \quad \text{with} \quad \chi = \frac{P_A}{P_L} , \tag{6}$$

where χ is an effective "stiffness" of the absorber against cw saturation. The stability relation (6) is visualized in Fig. 2(a). The tendency of a laser to Q-switch increases with the product $q_0 T_L$ and decreases if the saturable absorber is hard to saturate, i.e., $\chi \gg 1$. As can be inferred from Fig. 2(a) and Eq. (6), the laser can never Q-switch if

$$-2T_L P \frac{\mathrm{d}q}{\mathrm{d}P}\bigg|_{\mathrm{cw}} = \frac{2q_0 T_L}{\chi} < 1 . \tag{7}$$

Therefore, we define the expression (7) as the cw Q-switching driving force. For solid state lasers with long upper-state lifetimes, very small amounts of saturable absorption, even a fraction of a percent, may lead to a large enough cw Q-switching driving force (7) to Q-switch the laser. In principle, however, one can always leave the regime of Q-switching if the laser can be pumped sufficiently to saturate the absorber strongly. Unfortunately, the cw saturation power of an absorber is often higher than the damage threshold, so that the absorber cannot be bleached with cw radiation.

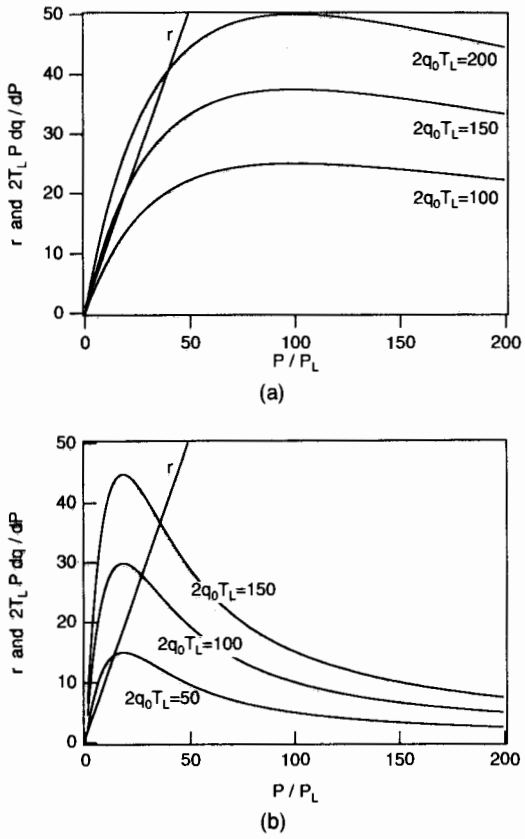

Fig. 2 Visualization of the stability relations for (a) cw Q-switching (5) and (b) Q-switched mode locking (15) for different products $2q_0 T_L$. The cw stiffness used for the plots is $\chi = 100$, and the pulsed stiffness $\chi_P = 10$, which corresponds to $T_A = 0.1$. The functional form of the two relations is very similar. The change in the stiffness when going from cw to pulsed saturation thus essentially rescales the x axis. For low-temperature-grown absorbers T_A can be as short as 10^{-3}, which changes the scale of the x axis by three orders of magnitude on going from cw saturation to pulsed saturation.

There is a tradeoff: On one hand the cw Q-switching driving force has to be small enough to prevent self-Q-switching, and on the other hand the saturable absorption has to be large enough so that mode locking is self-starting. The issue of self-starting of mode locking in lasers is still a topic of current research.[12–15] Many processes in a laser, such as spatial hole burning and dispersion, can inhibit[14] or promote[8] the self-starting of mode locking. However, their limiting effects on self-starting play a minor role if we can use a sufficiently strong saturable absorber.

2.2 *Self-Starting of Mode Locking Due to a Saturable Absorber*

We consider only one mechanism for self-starting of mode locking, which is in our case the dominant mechanism. In an ideal homogeneously broadened laser without any spatial hole burning and without a saturable absorber, only one longitudinal cavity mode at the center of the gain is running, and it saturates the gain, so that all neighboring modes are below threshold. Due to the saturable absorber, two-mode

coupling[16] between the cavity mode at line center and the cavity mode m times the mode spacing $2\pi/T_R$ away from the line center occurs. This two-mode coupling provides additional gain for adjacent modes to reach threshold. The growth rate of these modes can be derived from Eqs. (18) to (20) of Ref. 4 and becomes in our notation

$$\frac{1}{T_{\text{mod}}}=\left[\frac{2q_0}{(1+P/P_A)^2+(2\pi mT_A)^2}\frac{P}{P_A}\right.$$

$$\left.-\frac{2g_0}{(1+P/P_L)^2+(2\pi mT_L)^2}\frac{P}{P_L}\right]_{\text{cw}} . \tag{8}$$

Here $T_{\text{mod}}=\tau_{\text{mod}}/T_R$, if positive, is the buildup time of neighboring modes normalized to the round-trip time. For a short normalized recovery time of the absorber (i.e., $2\pi mT_A \ll 1$) and a long upper-state lifetime (i.e., $T_L \gg 1+P/P_L$), we can simplify Eq. (8) for a large number of neighboring modes and obtain for small cw saturation of the absorber the approximate condition

$$\frac{1}{T_{\text{mod}}}=\frac{2q_0}{(1+P/P_A)^2}\frac{P}{P_A}-\frac{2g_0}{(2\pi mT_L)^2}\frac{P}{P_L}$$

$$\approx\left[\frac{2q_0T_L}{\chi}-\frac{2g_0}{(2\pi m)^2T_L}\right]\frac{P}{P_LT_L} . \tag{9a}$$

Thus, despite the fact that the absorber is too weak to lead to cw Q-switching [see Eq. (7)], it can easily be strong enough to excite neighboring modes. These neighboring modes grow until a new steady state is reached. With sufficiently large saturable absorption we can neglect effects such as dispersion (i.e., unequal cavity mode spacing) and spatial hole burning, which lead to frequency pushing and pulling of the individual cavity modes. The threshold for mode locking will be reached when the growth rate (8) is positive. Far above the threshold for mode locking, the mode-locking buildup time will be proportional

$$\frac{1}{T_{\text{mod}}}\approx\left(\frac{2q_0T_L}{\chi}\right)\frac{P}{P_LT_L}\approx -2P\frac{dq}{dP} , \tag{9b}$$

which has been checked experimentally.[17] Naively one would think that when Eq. (8) is positive and the absorber is hard enough to saturate so that Eq. (5) is satisfied, the laser would always be stable against Q-switching and would run purely cw mode locked. However, what is most often observed experimentally is a train of mode-locked pulses under a Q-switched envelope (Fig. 3), referred to as Q-switched mode locking.

2.3 *Parameter Ranges for Q-Switched Mode Locking*

To understand the regime of Q-switched mode locking we reconsider the rate equations (1) to (3). Figure 3 indicates that we can approximate the laser power as

$$P(T,t)=E_P(T)\sum_n f(t-nT_R)$$

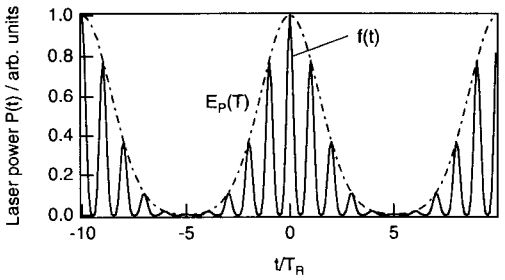

Fig. 3 Time dependence of the power when the laser operates in the Q-switched mode-locked regime.

$$\text{with} \int_{-T_R/2}^{T_R/2} f(t-nT_R)\,dt=1 , \tag{10}$$

where $E_P(T=nT_R)$ is the pulse energy of the nth pulse, which only changes appreciably over many cavity round trips, and $f(t)$ is the shape of the mode-locked pulses, which is not of interest for the time being. For simplicity we assume that the mode-locked pulses are much shorter than the recovery time of the absorber. In this case, the relaxation term for the absorber in Eq. (4) can be neglected for the duration of the mode-locked pulses. Since the absorber recovery time is assumed to be much shorter than the cavity round-trip time, the absorber is unsaturated before the arrival of a pulse. Thus, we obtain for the saturation of the absorber during one pulse

$$q(T,t)=q_0\exp\left[-\frac{E_p(T)}{E_A}\int_{-T_R/2}^{t} f(t')\,dt'\right] . \tag{11}$$

Therefore, the loss in pulse energy per round trip can be written as

$$q_p(T)=\int_{-T_R/2}^{T_R/2} f(t)q(T,t)\,dt=q_0\frac{1-\exp[-E_P(T)/E_A]}{E_P(T)/E_A} . \tag{12}$$

Equation (12) shows that the saturable absorber essentially saturates with the pulse energy, and not with the average intensity of the laser as before in the case (4) of cw Q-switching. Therefore, the absorber is much more strongly bleached at the same average power. After averaging of Eqs. (1) and (2) over one round trip, we obtain the following two equations for the dynamics of the pulse energy and the gain on a coarse-grained time scale T:

$$T_R\frac{dE_P}{dT}=2[g-l-q_P(E_P)]E_P , \tag{13}$$

$$T_R\frac{dg}{dT}=-\frac{g-g_0}{T_L}-\frac{gE_P}{E_L} . \tag{14}$$

The averaging is allowed because the saturation of the gain medium within one pulse is negligible due to the small interaction cross section of the solid state laser material. Comparing Eqs. (1), (2), and (4) with (12), (13), and (14), it becomes obvious that the stability criterion (5) applies also to Q-switched mode locking if we replace the formula (4) for

cw saturation of the absorber by the formula (12) for pulsed saturation. Then we have

$$-2E_P\frac{dq_p}{dE_P}\bigg|_{\text{cw mod}}<\frac{r}{T_L}\bigg|_{\text{cw mod}} \tag{15}$$

with

$$-2E_P\frac{dq_p}{dE_P}\bigg|_{\text{cw-mod}}=2q_0\frac{1-\exp(-E_P/E_A)\ (E_P/E_A+1)}{E_P/E_A}\ , \tag{16}$$

or again expressed in terms of the average power $P=E_P/T_R$, similar to Eq. (6), we obtain

$$-2T_LE_P\frac{dq_p}{dE_P}\bigg|_{\text{cw-mod}}$$

$$=2T_Lq_0\frac{1-\exp(-P/\chi_PP_L)\ (P/\chi_PP_L+1)}{P/\chi_PP_L}\ , \tag{17a}$$

where $\chi_P=\chi T_A$ describes an effective stiffness of the absorber compared with the gain when the laser is cw mode locked at the same average power as the cw laser. Thus, similarly to the case of cw Q-switching, it is useful to introduce the driving force for Q-switched mode locking:

$$-2T_LE_P\frac{dq_p}{dE_P}\bigg|_{\text{cw}}=\frac{2q_0T_L}{\chi_P}\ . \tag{17b}$$

Comparing Eqs. (7) and (17b), it follows that in the case of cw mode locking the absorber is saturated more strongly by a factor of $1/T_A$, which can easily be as large as 1000. Therefore, the tendency for Q-switched mode locking is significantly higher than for cw Q-switching. However, it becomes much easier to saturate the absorber strongly with an average power well below the damage threshold of the absorber [Fig. 2(b)]. In going from Fig. 2(a) to 2(b) we used $T_A=0.1$. We see that the short normalized recovery time essentially leads to a scaling of the abscissa when going from Fig. 2(a) to 2(b) and keeping all other parameters constant. Therefore, in the strong saturation limit of the saturable absorber, we can design a saturable absorber that both produces a high mode-locking driving force (9) to start the mode locking and is stable against Q-switching, since the "pulsed stiffness" of the absorber is much lower.

The theory presented so far yields guidelines for the design of an absorber that prevents Q-switching instabilities but still self-starts mode locking. A saturable absorber alone can shorten a pulse until it is roughly on the order of the absorber relaxation time if, of course, the gain bandwidth is sufficiently large. The pulse formation process is essentially given by the fast-saturable-absorber mode-locking model analyzed by Haus et al.[18] This is the case for picosecond lasers where dispersion and self-phase-modulation are not the dominant pulse-shaping mechanisms. In the next section we discuss a different mode-locking regime where an absorber with a relaxation time much longer than the pulsewidth is nevertheless responsible for short-pulse generation. Thus an absorber with a picosecond recovery time may even allow femtosecond-pulse generation. Or, as is the case in our bitemporal semiconductor absorbers, a fast time constant of the order of 100 fs may even allow ultrashort pulse generation below 10 fs.

3 Soliton Mode Locking

For ultrashort-pulse generation, a fast saturable absorber[19] [Fig. 4(a)], e.g., APM or KLM,[18] or the interplay between a slow saturable absorber and gain saturation [Fig. 4(b)], e.g., CPM dye lasers,[20] is usually used. Both mechanisms open a window of net gain, such that only the pulse itself experiences gain per round trip. This allows the system to discriminate against noise that may grow in the wings of the pulse, and therefore the pulse is kept stable against perturbations or noise.

Many experiments in the past have shown that soliton pulse shaping—the combined action of negative group-velocity dispersion (GVD) and self-phase-modulation (SPM)—may lead to additional pulse shortening and stabilization in actively and passively mode-locked lasers.[21,22] Recently, we have shown both theoretically and experimentally that solitonlike pulse formation in actively mode-locked lasers[23,24] allows considerable pulse shortening beyond that due to the usual active mode locking. In addition, an extension of this theory predicts that in the presence of solitonlike pulse shaping even a slow saturable absorber with a recovery time much longer than the pulsewidth can stabilize the pulse [Fig. 4(c)].[25] This is in contrast to the traditional picture that the gain window has to be closed immediately before and after the passage of the pulse. That is unnecessary in the soliton regime, because for the soliton the nonlinear effects due to SPM and the linear effects due to the negative GVD are in balance. In contrast, the noise or instabilities that might grow within the longer time window are not intense enough to experience the Kerr nonlinearity and are therefore spread in time. When they spread in time they experience the higher absorption due to the slowly recovering absorber after passage of the much shorter solitonlike pulse. Thus the instabilities see less gain per round trip than the soliton and will decay with time. A detailed theoretical justification of this simple picture can be found in Ref. 25. In this paper we present only a brief discussion of the results.

For femtosecond pulse generation we have to extend our laser model to include SPM and GVD; see Fig. 5. We can describe the laser by Haus's master equation of mode locking[19]

$$T_R\frac{\partial}{\partial T}A(T,t)=\left(-iD\frac{\partial^2}{\partial t^2}+i\delta|A(T,t)|^2\right)A(T,t)$$

$$+\left(g-l+D_g\frac{\partial^2}{\partial t^2}-q(T,t)\right)A(T,t)\ , \tag{18}$$

where $A(T,t)$ is the slowly varying field envelope of the pulse, D the intracavity GVD, $D_g=g/\Omega_g^2$ the gain dispersion, δ the nonlinear coefficient due to SPM, and l the amplitude loss and g the gain as before. Here Ω_g is the HWHM gain bandwidth. Equation (18) describes the laser dynamics on two time scales: T, which is on the order of the round trip time in the laser cavity and which we have already introduced in Sec. 2, and t, which is on the order of the pulse width and

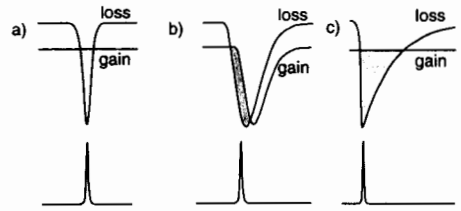

Fig. 4 Pulse shaping mechanism due to gain and loss dynamics in a mode-locked laser using (a) a fast saturable absorber only, (b) a slow saturable absorber plus slow gain saturation, (c) a slow saturable absorber and soliton formation.

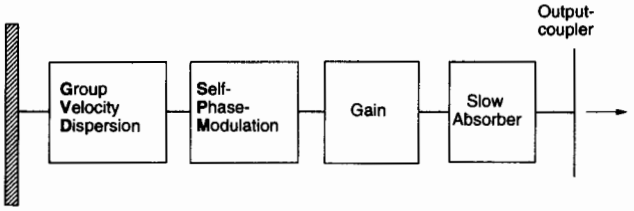

Fig. 5 The most important intracavity elements of a passively mode-locked laser. The action of each physical element in the cavity on the pulse per round trip can be described mathematically by a differential or integral operator. If the changes per round trip are small, we simply can add up all these operators, and the sum then describes the change in the pulse over one round trip as expressed in Eq. (18).

which resolves the pulse shape. Since we are now explicitly interested in pulse shaping, we have to treat the action of the saturable absorption $q(t)$ on the short time scale:

$$\frac{\partial q(T,t)}{\partial t} = -\frac{q-q_0}{\tau_A} - \frac{|A(T,t)|^2}{E_A} q \ , \tag{19}$$

where we have again assumed that the recovery time τ_A of the saturable absorber is much shorter than the round-trip time of the pulse, so that the absorber recovers completely between two consecutive pulses. The first part of Eq. (18) is the nonlinear Schrödinger equation, which has the well-known fundamental soliton solution

$$A_s(T,t) = \sqrt{\frac{W}{2\tau}}\ \mathrm{sech}\left(\frac{t}{\tau}\right) \exp\left(i\Phi_0 \frac{T}{T_R}\right)$$

$$\text{with } \Phi_0 = \frac{\delta W}{4\tau} = \frac{|D|}{\tau^2} \ , \tag{20}$$

where W is the pulse energy, Φ_0 is the phase shift of the soliton per round trip in the cavity, and the FWHM pulse width is given by $\tau_{\mathrm{FWHM}} = 1.76\tau$. As we have seen in the last section, the laser is stable against Q-switching if the absorber is saturated strongly enough when operating in pulsed mode. For simplicity we therefore assume that the saturation energy of the saturable absorber is much smaller than the energy of the soliton, i.e., $W \gg E_A$. Then the soliton saturates the absorber completely, and we obtain for the energy balance from Eqs. (18) and (20) in steady state $g = l + D_g/(3\tau^2)$. Thus the pulse sees additional losses due to the finite gain bandwidth only. In contrast to the soliton, the continuum, which is spread by GVD in time, experiences additional losses when passing the slowly recovering absorption saturated by the soliton $q(t) = q_0[1 - \exp(-t/\tau_A)]$, as is shown in Fig. 6. The solitonlike pulse is stable as long as the soliton sees less loss than the continuum and therefore can saturate the gain to a level where the continuum is below threshold. Approximating the exponential response by a V-shaped response allows for an estimate of the pulse width of the shortest soliton that can still be stabilized by the absorber[25]:

$$\tau = \left(\frac{1}{\sqrt{6}\Omega_g}\right)^{3/4} \left(\frac{\tau_A g^{3/2}}{q_0}\right)^{1/4} (\Phi_0)^{-1/8} \ . \tag{21}$$

This qualitative result clearly shows that we can exploit a considerable part of the available gain bandwidth even with a slow absorber, i.e., $\tau_A \gg \Omega_g^{-1}$. Thus soliton mode locking allows us to produce considerably shorter pulses than the recovery time of the absorber. A factor of 20 can easily be reached.[25] Our stability analysis for Q-switched mode locking presented in Sec. 2 therefore is fully justified on the assumption that the pulses are much shorter than the recovery time of the absorber.

4 The Antiresonant Fabry-Perot Saturable Absorber for Controlling the *Q*-Switching and Mode Locking in Solid State Lasers

In the preceding sections, the parameter ranges for Q-switching, cw mode locking, and Q-switched mode locking have been discussed. Given a laser with the key parameters intracavity pulse energy, loss, small-signal gain, upper-state lifetime of the laser material, and its saturation energy, it is important to be able to adjust the parameters of the absorber according to the conditions derived in Sec. 2 in order to obtain stable, self-starting cw mode locking or, if desired, operation in any other regime. In this section, we show how this can

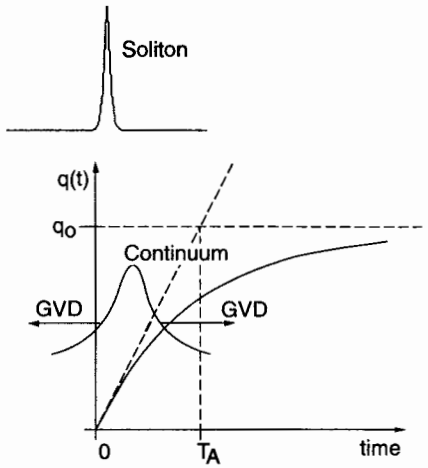

Fig. 6 We assume that the energy of the soliton is much larger than the saturation energy of the absorber. Thus the soliton saturates the absorber completely and immediately after arrival at the absorber. The background radiation (continuum), which competes with the soliton for the available gain, is stretched in time by GVD and therefore experiences high loss in the absorber. This process stabilizes the soliton against the continuum and leads to stable and clean solitonlike pulses.

be achieved with our semiconductor antiresonant Fabry-Perot saturable absorbers (A-FPSA). Antiresonance means that the intensity inside the Fabry-Perot is smaller than the incident intensity, which decreases the device loss and increases the saturation intensity. The damage threshold is then determined by the top reflector, which is typically an evaporated dielectric mirror similar to other mirrors inside the laser cavity.

4.1 *Device Structure*

In practical use, the AFPSA is a nonlinear mirror, typically ≈400 μm thick, which simply replaces one of the laser cavity mirrors to passively mode-lock a cw-pumped laser. The nonlinear reflectivity change in the AFPSA is due to band filling where the absorption is bleached with the photoexcited carriers because of the Pauli exclusion principle. The impulse response shows a bitemporal behavior, i.e., a slow time constant due to carrier recombination for efficient starting of the mode locking and the generation of picosecond pulses as described in Sec. 2, as well as a fast time constant due to carrier thermalization for further pulse shortening and sustaining of sub-100-fs pulses according to Sec. 3.

The samples we have built use a bottom mirror that consists of 16 to 25 pairs of (Al)GaAs and AlAs quarterwave layers forming a Bragg mirror with a center wavelength of either 830 nm (for Cr:LiSAF) or 1050 nm (for Nd-doped crystals or glasses) and approximately 100-nm bandwidth (see Fig. 7). On top of the mirror, the absorber is grown, consisting of bulk (Al)GaAs for operation below 870 nm or a strained InGaAs-GaAs superlattice for operation at 1050 nm, where the indium content in the wells determines the absorption edge, which can be varied from 900 nm to potentially 2 μm. Finally, a top mirror consisting of three or four pairs of SiO_2 and TiO_2 quarterwave layers is evaporated on top of the absorber.

In addition, the absorber is grown at low temperatures (i.e., between 200 and 400°C instead of[9,10] >600°C). The advantages of low-temperature MBE growth are twofold: First, incorporation of excess arsenic in the form of interstitials and clusters leads to interband states, which drastically reduce the lifetime of photogenerated carriers and thus the absorber recovery time—an essential parameter for the mode-locking performance[23]; see also Eqs. (4) and (21). It has been shown that this lifetime depends on the growth temperature in a very controlled and reproducible manner. Second, the degradation in surface morphology of strained InGaAs-GaAs multiple quantum wells (MQWs) using normal growth conditions, which would result in high scattering losses, are reduced, since the defects have dimensions much smaller than the optical wavelength and no cross-hatched roughness is present in our low-temperature-grown MQWs.

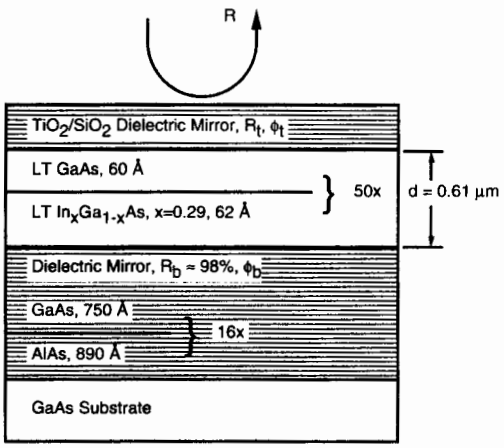

Fig. 7 Structure of an antiresonant Fabry-Perot saturable absorber (A-FPSA) designed for an operation wavelength of ≈1 μm. For operation at 800 nm, an AlGaAs bulk absorber was used.

4.2 *Experimental Determination of the Absorber Parameters*

For the measurements, we used both InGaAs MQW samples and bulk (Al)GaAs samples MBE-grown at different substrate temperatures but otherwise identical, with the top mirror replaced by an antireflection (AR) coating. The low-intensity reflectivity (shown in Fig. 8(a) for the InGaAs samples) has been measured absolutely with a Varian Cary 5E spectrophotometer using the VW calibration method. All curves show a dip near 1050 nm due to the exciton resonance, which broadens for lower growth temperatures. The minima above 1100 nm and below 1000 nm are caused by the bandwidth of the bottom mirror. The reflectivity of three corresponding A-FPSAs (i.e., with a highly reflecting top mirror) is shown in Fig. 8(b). As expected, the reflectivity is close to unity at antiresonance, but a slight variation due to the varying absorption can still be seen. The sharp minima near 1100 and 1000 nm are resonances. The useful spectral range in all three samples is > 100 nm. The AlGaAs samples at 830 nm showed very similar low-intensity reflectivities.

The absorber recovery time has been determined with a standard degenerate noncollinear pump-probe experiment, with perpendicular polarization of pump and probe to eliminate coherent artifacts, using 100-fs pulses from a Ti-sapphire laser. The probe beam was strongly attenuated compared to the pump beam. We also used a low-duty-cycle (1 : 20) acoustic-optic modulator to gate the pump and probe beams in order to eliminate heating effects. Figure 9(a) shows a typical bitemporal impulse response of an InGaAs sample grown at 260°C for different pump pulse energies and a wavelength of 1060 nm. The first, fast decay constant, on the order of 200 fs, is due to intraband thermalization, and the subsequent slower time constant is associated with carrier recombination. Since the slow time constant determines the cw saturation intensity, it is important in the picosecond and mode-locking buildup regime. The carrier lifetimes of different samples are summarized in Fig. 9(b). The dependence on the growth temperature is evident. It is thus possible to choose a lifetime τ_A from several picoseconds up to several tens of picoseconds simply by adjusting the growth temperature. The upper limit for the growth temperature for the case of the strained InGaAs system is progressively reduced with increased lattice mismatch (i.e., increased In concentration) by the onset of cross-hatched roughness, leading to high, nonsaturable scattering losses.[26,27] In the case of the unstrained AlGaAs system, there is no such limitation, and the lifetime can be as long as 1 ns for normal growth temperature, which is close to the round-trip time in typical lasers.

The saturation fluence E_A^0 of the material has been determined from the measured average reflectivity as a function of incident pulse energy density on the AR-coated

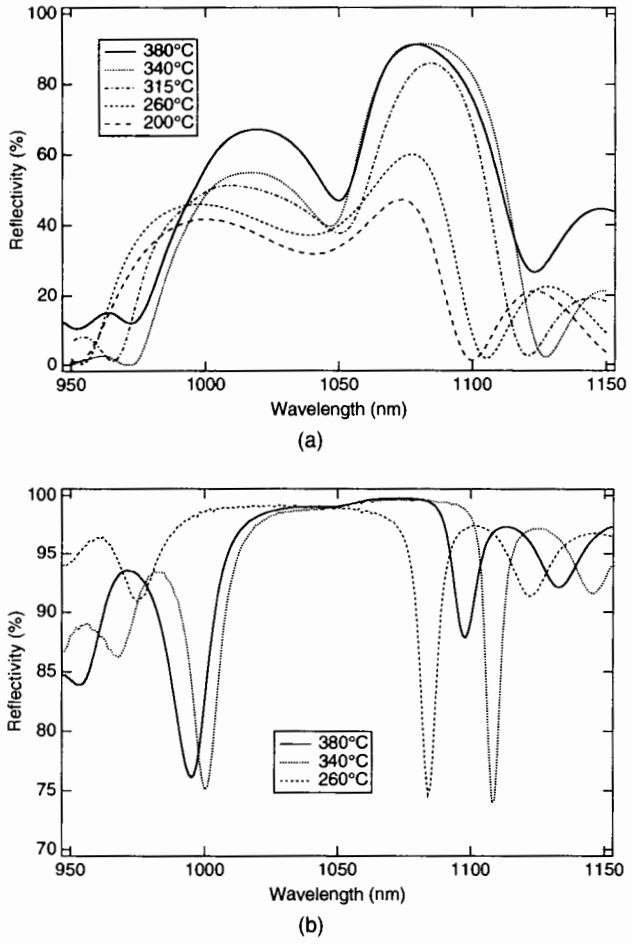

Fig. 8 Low-intensity reflectivity of (a) AR-coated samples and (b) A-FPSAs grown at different temperatures.

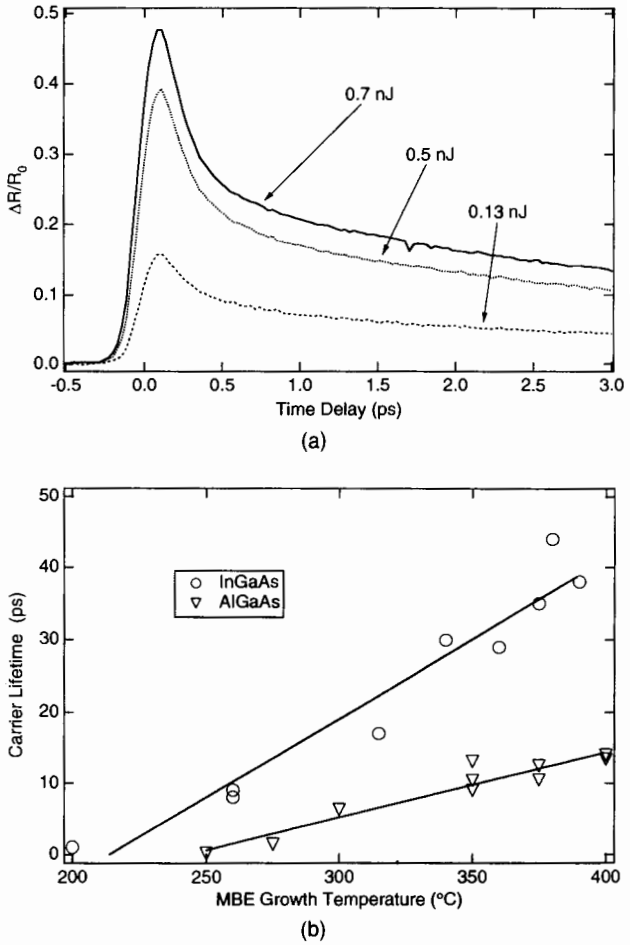

Fig. 9 (a) Typical bitemporal pulse response of the sample grown at 260°C for varying pulse energy (0.13, 0.5, 0.7 nJ; $\lambda = 1060$ nm); (b) measured carrier lifetimes versus growth temperature.

samples [Fig. 10(a)]. We also introduce R_{ns} to describe the non-saturable part of the losses α_{ns}, i.e., $R_{ns} = R(E_{in} \to \infty) = \exp(-4\alpha_{ns} d)$. Included in R_{ns} are the reflectivity of the bottom mirror R_b, scattering losses due to impurities at the surface of the sample, and losses introduced by free-carrier absorption. The measured data have been fitted with a calculated function derived from a traveling-wave rate-equation model[17,28,29] to obtain the fitting parameters E_A^0 and $\Delta R_{ns} \equiv 1 - R_{ns}$. For an AR-coated sample and for the case where the pulse duration is much shorter than the recovery time of the absorber, we obtain for the energy reflectivity

$$R(E_{in}) = \frac{E_{out}}{E_{in}} = R_{ns} \frac{\log\left(\frac{R_0 - 1}{R_f - 1}\right)}{\log\left(\frac{R_0 - 1}{R_f - 1}\right) - \log\left(\frac{R_0}{R_f}\right)}, \tag{22}$$

where we have introduced the unsaturated low-intensity reflectivity R_0 and the final reflectivity after the passage of a pulse with the fluence E_{in}:

$$R_f = \frac{R_0}{R_0 - (R_0 - 1)\exp(-E_{in}/E_A^0)}. \tag{23}$$

We used (22) and (23) to fit the experimentally measured $R(E_{in})$ in order to obtain E_A^0 and R_{ns} and to calculate the corresponding reflectivity of the A-FPSA [Fig. 10(a)].

The results for different samples are summarized in Fig. 10(b). The saturation fluences and the nonsaturable losses for $\lambda = 1040$ nm and $\lambda = 1060$ nm are depicted as a function of growth temperature. As expected, the nonsaturable losses increase for decreasing growth temperature, but their influence is strongly reduced for an A-FPSA with a high top reflector. However, they reduce the total amount of nonlinear reflectivity change that can be achieved. The parameter E_A^0 also shows an increase for decreasing growth temperature due to a reduction of the absorption cross section.

The measurements at different wavelengths (1000, 1020, 1040, 1060 nm) showed, as expected, a higher saturation fluence for shorter wavelengths (i.e., 137, 97, 50, 45 μJ/cm^2, respectively, for the sample with a growth temperature of 315°C, and similar for the others), which results in smaller nonlinearities at shorter wavelengths. In general, however, the variation of the saturation fluence in the region of interest (i.e., between 1040 and 1060 nm) is on the order of only a few percent [Fig. 10(b)].

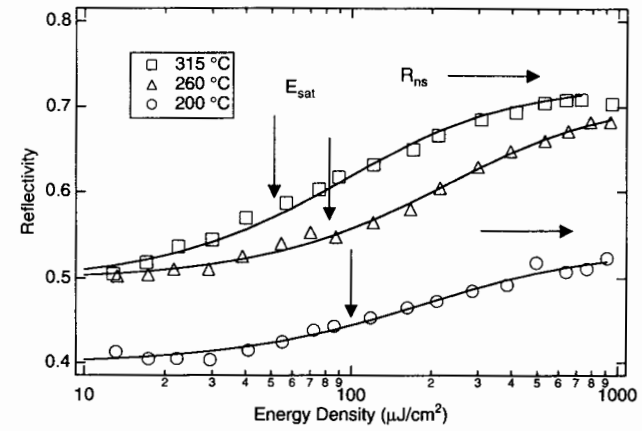

(a)

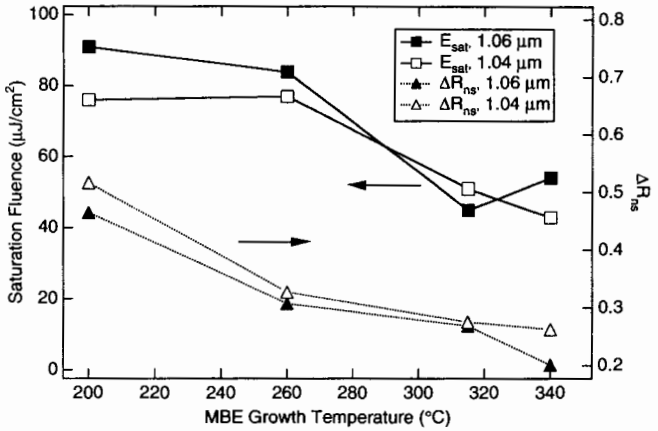

(b)

Fig. 10 (a) Measured change in reflectivity versus pulse energy density (symbols) and theoretical fit (solid lines); (b) saturation fluence and nonsaturable losses for samples grown at different temperatures.

4.3 *Operation and Design Criteria for the Saturable-Absorber A-FPSA*

In Ref. 17, a detailed discussion of the operation of an A-FPSA has been given. Based on the measured material parameters of samples with an AR coating as discussed in the previous section, the saturation behavior of corresponding A-FPSAs with a highly reflecting top mirror can be derived. The most important point is that the thickness of the absorbing layer is designed so that the laser wavelength is at an antiresonance of the Fabry-Perot resonator. In contrast to the sharp resonance, the antiresonance in a high-finesse Fabry-Perot resonator is a broad maximum of the reflectivity as a function of wavelength [see Fig. 8(b)]. The reflectivity of the unsaturated A-FPSA at antiresonance can be calculated from well-known Fabry-Perot formulas as

$$R_{\mathrm{FP}}=\frac{[\sqrt{R_t}+\sqrt{R_b}\,\exp(-2\alpha d)]^2}{[1+(R_tR_b)^{1/2}\,\exp(-2\alpha d)]^2} \tag{24}$$

with the unsaturated amplitude absorption coefficient α.

The measurement of the saturation fluence has been performed on AR-coated samples. In a Fabry-Perot resonator at antiresonance the ratio between the intensity inside and outside the resonator is given by

$$I_{\mathrm{HR}}=\xi I_{\mathrm{AR}} \tag{25}$$

with the reduction factor

$$\xi=\frac{1-R_t}{[1+(R_tR_b)^{1/2}\,\exp(-2\alpha d)]^2}\ . \tag{26}$$

Therefore, the effective saturation fluence of the A-FPSA is

$$E_A^{\mathrm{eff}}=\frac{1}{\xi}E_A^0\ . \tag{27}$$

For our A-FPSAs, we calculated for ξ a value of typically between 0.007 and 0.02, depending on the top reflector. Equations (26) and (27) already show that one of the main advantages of the A-FPSA is the possibility of varying the saturation fluence just by using a different top reflector.

The corresponding reflectivity change of the A-FPSA follows directly by replacing the term $\sqrt{R_b}\,\exp(-2\alpha d)$ in Eq. (24) with the effective saturated value $[R(\xi E_{\mathrm{in}})]^{1/2}$ obtained from Eq. (22) and obtain at antiresonance for the energy reflectivity

$$R_{\text{A-FPSA}}(E_{\mathrm{in}})=\frac{\{\sqrt{R_t}+[R(\xi E_{\mathrm{in}})]^{1/2}\}^2}{\{1+[R_tR(\xi E_{\mathrm{in}})]^{1/2}\}^2}\ . \tag{28}$$

Now E_{in} is the incident pulse fluence (or energy, when multiplied by the effective spot size $A_{\mathrm{eff},A}$ on the A-FPSA), and the factor ξ from Eq. (26) allows for the reduction of the intensity inside the absorber.

To make connection with the theory of saturable-absorber mode locking and Q-switching as presented in Sec. 2, we have to express the saturable absorption per round trip in Eqs. (5), (8), (15) by the explicit expression for the A-FPSA derived in this section. Since we are always working in the limit of small changes per pass, i.e., small saturable loss per round trip, we obtain for the case of pulsed saturation from (28)

$$2q(E_P)=1-R_{\text{A-FPSA}}(E_P)\ . \tag{29}$$

To discuss the mode-locking buildup regime and cw Q-switching, we have to consider the saturation of the A-FPSA for cw intensities. Equation (28) cannot be used in this case, since it describes the pulsed saturation. The cw saturation intensity is related to the pulsed saturation fluence by

$$I_A=\frac{E_A^0}{\tau_A} \tag{30}$$

and is inversely proportional to the recovery time τ_A. The derivative of the reflectivity with respect to the intensity is directly related to the mode-locking driving force or mode-locking buildup time [see Eqs. (7) and (9b)] and is given by[17]

$$\left(\frac{dR_{\text{A-FPSA}}^{\mathrm{cw}}}{dI}\right)_{I=0}\approx\frac{\tau_A(1-R_t)^2}{E_A^0}$$

$$\times\frac{[1-\exp(-2\alpha_0 d)\,\exp(-2\alpha_{ns}d)}{[1+\exp(2\alpha_0 d)][1+\exp(-2(\alpha_0+\alpha_{ns})d)]^2}\,, \tag{31}$$

assuming both R_b and R_t are close to unity. For our samples, we obtained for Eq. (31) values on the order of 10^{-11} cm^2/W, which is typically three orders of magnitude larger than the driving force due to Kerr lensing, even if the laser is operated close to the limits of the stability regime.[17] This explains why an A-FPSA efficiently starts passive mode locking. From Eq. (31) we obtain for the mode-locking driving force (9b)

$$-2P\left(\frac{dq}{dP}\right)_{P=0}\approx P\frac{\tau_A(1-R_t)^2}{E_A^0 A_{eff,A}}$$

$$\times\frac{[1-\exp(-2\alpha_0 d)]\,\exp(-2\alpha_{ns}d)}{[1+\exp(2\alpha_0 d)]\{1+\exp[-2(\alpha_0+\alpha_{ns})d]\}^2}\,. \tag{32}$$

According to Eq. (7), this mode-locking driving force is also responsible for cw Q-switching.

We are now able to draw several conclusions for the design of an A-FPSA. The parameters that can be varied to adapt the absorber to the requirements of a solid state laser are the material parameters α_0, E_A^0, and τ_A as well as the device parameters R_t (i.e., the number of dielectric layer pairs), the thickness d of the absorber, and the spot size $A_{eff,A}$ on the A-FPSA. The material parameters can be adjusted within a certain range by varying the growth temperature (E_A^0 and τ_A) and the indium or aluminum content or the quantum well thickness (α_0). The reflectivity of the bottom reflector should in any case be as close to 100% as possible, since any reduction contributes to the nonsaturable losses. This is, however, typically not critical, since the influence of R_b on the insertion losses is strongly reduced in an A-FPSA with a high-reflectivity top mirror. Increasing the thickness d has the same effect as increasing α_0: an increase in losses and a weak increase in ξ (thus a weak decrease of the effective saturation fluence E_A^0/ξ and increase of the driving force d R/dI). The same can be achieved by decreasing the top reflectivity R_t. So there is the tradeoff that increasing the driving force leads to an increase in intracavity losses. With our LT-grown semiconductor absorbers, however, we have the additional possibility of increasing the driving force by increasing the carrier lifetime or by reducing the spot size on the A-FPSA without affecting the losses.

Table 1 Extracted absorber and laser parameters for the Q-switching experiments with different A-FPSAs. The additional parameters, which were the same for all experiments, are $E_L=60$ μJ; $T_R=3.85$ ns; $T_L=117\times10^3$; the effective area on the absorber, $A_{eff,A}=3.7\times10^{-5}$ cm^2; and the mode size in the laser crystal, $A_{eff,L}=11\times10^{-5}$ cm^2.

Growth temp.	τ_A [ps]	R_0	R_∞	E_A^0 [μJ/cm^2]	ξ	E_A [nJ]	χ ·10^3	χ_P	E_P [nJ]	$x_P=E_P/E_A$	τ_P [ps]
260 °C	3.8	0.4	0.68	79	0.015	188	370	370	-	-	-
315 °C	15	0.37	0.73	51	0.016	118	60	232	43	0.36	10.6
340 °C	22	0.41	0.74	45	0.015	108	37	212	58	0.54	9.5
380 °C	40	0.48	0.79	67	0.014	171	32	337	40	0.23	11.4

5 Experimental Results

Samples from the same epitaxial runs with top-mirror reflectivities of 96% ± 0.5% have been used as A-FPSAs in various mode-locking experiments with Nd:YAG, Nd:YLF, and Nd:glass lasers.[6] In this section we first investigate experimentally the Q-switching and mode-locking buildup criteria derived in Sec. 2. Then we present a Cr:LiSAF laser where the A-FPSA self-starts and sustains 45-fs solitonlike pulses according to the theory in Sec. 3.

5.1 *Experimental Characterization of the Q-Switching and Self-Starting of Picosecond Lasers Using an A-FPSA*

To demonstrate the validity of the Q-switching and self-starting criteria developed above, we built a Nd:YLF laser with the gain medium in the middle of the cavity[6] to minimize effects due to spectral hole burning.[8] The absorber parameters used in the experiment can be extracted from the figures of Sec. 4 and are summarized together with the laser parameters in Table 1. Since the A-FPSA is much more complex than the simple two-level saturable-absorber model used in Sec. 2, we have to consider many more parameters for a detailed quantitative description. However, to obtain a quick overview of the laser dynamics implied by the A-FPSA, it is very useful to compute the key parameters of the equivalent simple two-level absorber model. The maximum amount of saturable absorption is $2q_0\approx\xi(R_{ns}-R_0)\approx0.015\times0.3=0.0045$, where we have used average values from Table 1 for the corresponding parameters. The normalized upper-state lifetime of Nd:YLF in this cavity (Table 1) is very large: $T_L=117\times10^3$. However, the "stiffness" of the absorber for cw radiation is also very large, due to the high reflectivity of the top mirror of the A-FPSA. The stiffness has a typical value of $\chi\approx3\times10^4$ to 3×10^5, resulting in $2q_0T_L/\chi\approx2\times10^{-2}$ to 2×10^{-3}. Therefore, the laser is stable against cw Q-switching according to Eq. (7). However, due to the low-temperature growth, the carrier lifetime is roughly a factor of 100 to 1000 times shorter than the cavity round-trip time $T_R=3.8$ ns, which reduces the stiffness against pulsed saturation typically by a factor of 100 to 1000. This results in a pulsed stiffness of $\chi_P\approx212$ to 370 and a critical product of $2q_0T_L/\chi_P\approx2$. Therefore, some of these absorbers are close to the instability of Q-switched mode locking.

For a further quantitative discussion of the results we have to substitute the exact reflectivity function (28), (29) for the A-FPSA into the stability condition (15). The numerical evaluation of this stability condition for the different A-FPSAs is shown in Fig. 11 in terms of the pulsed stiffness χ_P of the A-FPSA and the pulsed saturation $x_P=E_P/E_A$. The experimentally determined transition points from the regime of Q-switched mode locking to pure cw mode locking are also shown. Comparing Table 1 with Fig. 11, we see that the 260°C sample, which shows the shortest carrier lifetime, the largest pulsed stiffness, and therefore the lowest mode-locking driving force (31), does not reach the threshold for

mode locking. All other samples, however, reach the threshold for self-starting of mode locking and only show Q-switched modelocking at lower pump powers. At larger pump powers, where the absorber is more strongly saturated, the regime of Q-switched mode locking can be overcome and we obtain pure cw mode-locked pulses. The pulse energies, the pulsed saturation, and the pulse width at which pure cw mode locking occurs are also summarized in Table 1. The agreement between experiment and theory in Fig. 11 is fairly good, considering the sensitivity of the transition curve between Q-switched mode locking and cw mode locking. Deviations of only 0.5% from the assumed top mirror reflectivity of 96% lead to a variation in the ordinate of the stability boundary by about 15%. In the future the theory derived in previous sections will allow for a redesign of the absorbers in such a way that the dependence of the laser dynamics on the actual device parameters is less critical. We see that in all cases the pulse width is shorter than the recovery time of the absorber, which is consistent with the assumptions made in our theory.

These results demonstrate that we can design an absorber that is completely stable against cw Q-switching but that self-starts the mode locking reliably and generates picosecond pulses with a pulse width of the order of the recovery time of the absorber. So far we have demonstrated the use of the semiconductor absorbers for the generation of picosecond pulses. However, as we have seen in Sec. 3, with the help of soliton formation in the laser we can even generate pulses much shorter than the response time of the absorber.

5.2 *50-fs Diode-Pumped Cr:LiSAF Laser*

Using two high-brightness laser diodes as pump sources, brightness-maintaining focusing optics, and an A-FPSA as a low-loss saturable absorber, we obtained self-starting 45-fs pulses (Fig. 12) with 60-mW average power mode-locked. This demonstrates the shortest pulse ever obtained from a diode-pumped Cr:LiSAF laser and improved output power over our previously published diode-pumped Cr:LiSAF work.[30] The shortest ever demonstrated Cr:LiSAF laser (33 fs) used a diffraction-limited pump source.[31]

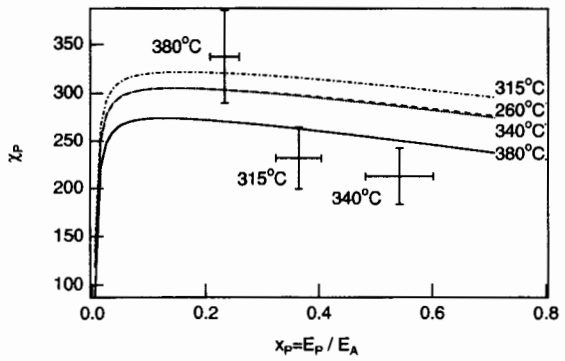

Fig. 11 The lines show the stability boundaries for Q-switched mode locking according to Eq. (15) for the A-FPSAs with parameters given in Table 1. Above the corresponding line the laser is stable against Q-switched mode locking. The measured transition points are the crosses, where the bars indicate the measurement errors of the stiffness and of the ratio between pulse and saturation energy. The 260°C A-FPSA did not show any mode locking or Q-switching, since the driving forces are too low due to its short absorber recovery time.

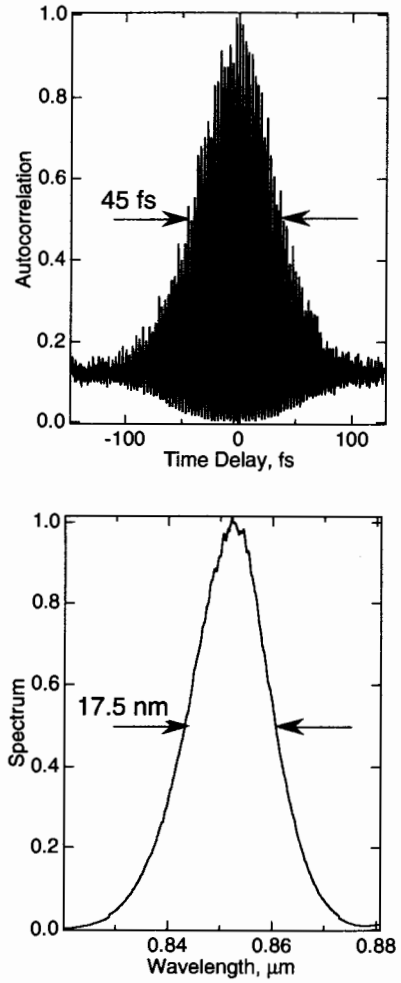

Fig. 12 Autocorrelation and pulse spectrum.

The laser cavity (Fig. 13) is a standard delta cavity, with a fused silica platelet (3 mm thick) in a second intracavity focus[32] and a curved mirror that focuses the laser mode onto the A-FPSA with a 15-μm radius. Two 400-mW-output-power diodes emitting from 100-μm stripes (Applied Optronics AOC-670-400) pumped the 1.5% Cr-doped crystal (Lightning Optical) from both sides with about 600 mW of total absorbed pump power. The pump beam was collected in its highly diverging direction by a single-axis collimating lens (Blue Sky SAC900, AR-coated at 700 nm), followed by two achromatic spherical lenses, which image the pump light into the laser crystal through a cavity mirror, providing mode matching to the laser mode over the ≈1-mm absorption depth of the crystal.[30]

Self-phase-modulation (SPM) in diode-pumped Cr:LiSAF lasers is usually low, leading to an equivalent soliton phase shift of $\Phi_0 < 0.005$ for 50 fs pulses according to Eq. (20), owing to both the low nonlinear refractive index n_2 of LiSAF and the large mode cross section required for mode-matching to the laser diode pump beam. The resulting soliton pulse shaping as described in Sec. 3 is very weak, limiting the achieved pulse durations to ≈100 fs, which can be attributed to the fast relaxation time of the saturable absorber.[30] Therefore, we introduced a glass platelet at an intracavity focus to increase SPM to $\Phi_0 \approx 0.07$, allowing us to achieve a pulse

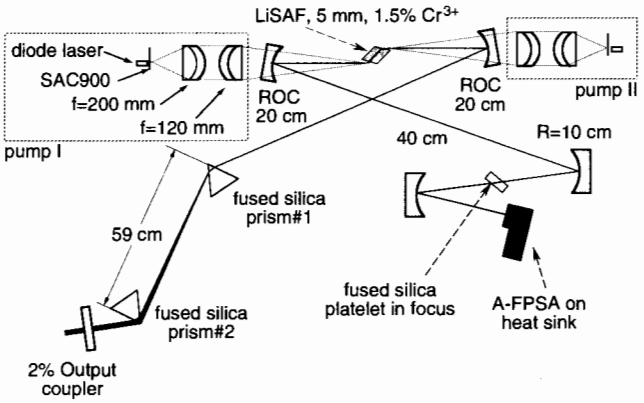

Fig. 13 Diode-pumped mode-locked Cr:LiSAF laser cavity.

width as short as 45 fs. In this case, SPM and GVD are clearly the dominating effects in pulse shaping, as opposed to gain dispersion and saturable absorption. From the discussion of the A-FPSA in Sec. 3 we know that the pulse shaping due to the saturable absorption is less than 0.5% per round trip. Thus, when the gain is saturated, all the amplitude effects per round trip are at least one order of magnitude smaller than the phase effects of GVD and SPM. This is additionally confirmed by the observation that the time-bandwidth product (0.32) is at the transform limit, indicating that the laser runs in the soliton regime. The GVD in our setup is estimated to be around $D = -50$ fs^2, which agrees well with the expected value from soliton theory.

The A-FPSA, with a bulk AlGaAs saturable absorber, can also provide for self-starting. On inserting it into the cavity, the laser goes into mode-locked operation spontaneously, The device can be positioned over practically the full stability range while still maintaining mode locking. As mode locking is not very sensitive to the exact position of either the A-FPSA or the glass platelet, Kerr-lensing effects are seen not to be required for mode locking. The very low linear insertion loss due to the A-FPSA is only 1 to 1.5%, allowing us to achieve an average output power of 60 mW using a 2% output coupler.

6 Conclusion

Starting from a simple two-level laser and absorber model, we have characterized the dynamics of solid state lasers mode-locked and Q-switched by the absorber. The unique properties of solid state laser materials, i.e., their long upper-state lifetime and their small cross sections for stimulated emission, allow for a separation of the laser dynamics on at least two time scales. One determining process is the energy buildup, which occurs typically on a time scale of the upper-state lifetime of the laser. The other process is the pulse shaping, which occurs within several round trips in the cavity. Separating these processes, we can distinguish between the different laser dynamics called cw Q-switching, Q-switched mode locking, and cw mode locking. We found the stability boundaries of the different regimes, which give us guidelines for the design of absorbers for a given solid state laser to favor one of these regimes.

Low-temperature-grown semiconductors are an excellent material for saturable absorbers to mode-lock lasers, since the carrier lifetime can be engineered to values well below typical round-trip times in solid-state-laser cavities. Insertion of this absorber material in a Fabry-Perot cavity results in an absorber with a large stiffness against cw-saturation, which prevents passive cw Q-switching but still self-starts mode locking. When the pulses become short enough, the laser saturates the absorber much more efficiently, which stabilizes the laser against undesired Q-switched mode locking. We demonstrated experimentally that this technique can control the laser dynamics of a large variety of solid state lasers in the picosecond regime. In addition, by exploiting the bitemporal behavior of the semiconductor devices and soliton formation due to negative GVD and SPM, we can use the same semiconductor absorbers to mode-lock the lasers in the femtosecond regime.

The saturable-absorber techniques demonstrated do not interrelate the spatial profile of the laser mode with the laser dynamics as is the case for Kerr-lens mode locking. Therefore, we believe that the saturable-absorber control of the laser dynamics as shown here is easily scalable to the new emerging high-power laser designs and will lead to less-restricted design tolerances in general.

Acknowledgment

This work was supported by the Swiss Priority Program in Optics and the Swiss National Fund No. 21-39362.93. Special thanks go to Lightning Optical for supplying the low-loss Cr:LiSAF crystal, to Heng Chiu from AT&T Bell Laboratories for some of the semiconductor saturable absorbers, and to M. Moser at the Paul Scherrer Institut Zürich for the broadband AlGaAs-AlAs bottom mirrors that were used for some of the Cr:LiSAF results.

References

1. A. Giesen, H. Hügel, A. Voss, K. Wittig, U. Brauch, and H. Opower, "Scalable concept for diode-pumped high-power solid-state lasers," *Appl. Phys. B* **58,** 363–372 (1994).
2. E. P. Ippen, "Principles of passive mode locking," *Appl. Phys. B* **58,** 159–170 (1994).
3. A. Penzkofer, "Passive Q-switching and mode-locking for the generation of nanosecond to femtosecond pulses," *Appl. Phys. B* **46,** 43–60 (1988).
4. H. A. Haus, "Parameter ranges for cw passive modelocking," *IEEE J. Quantum Electron.* **12,** 169–176 (1976).
5. U. Keller, D. A. B. Miller, G. D. Boyd, T. H. Chiu, J. F. Ferguson, and M. T. Asom, "Solid-state low-loss intracavity saturable absorber for Nd:YLF lasers: an antiresonant semiconductor Fabry-Perot saturable absorber," *Opt. Lett.* **17,** 505–507 (1992).
6. U. Keller, "Ultrafast all-solid-state laser technology," *Appl. Phys. B* **58,** 347–363 (1994).
7. A. E. Siegman, *Lasers,* University Science Books, Mill Valley, CA (1986).
8. B. Braun, K. J. Weingarten, and U. Keller, "Spatial-hole-burning-enhanced reduction of pulsewidth in modelocked end-pumped solid-state lasers," in *Conf. on Lasers and Electro Optics, Anaheim 1993, Technical Digest,* paper CTh1.
9. G. L. Witt, R. Calawa, U. Mishra, and E. Weber, Eds., *Low Temperature (LT) GaAs and Related Materials,* vol. 241 Pittsburgh (1992).
10. T. H. Chiu, U. Keller, M. D. Williams, M. T. Ason, and J. F. Ferguson, "Low-temperature growth of InGaAs/GaAs saturable absorbers for passively mode-locked solid-state laser applications," (submitted for publication).
11. H. Haken, *Synergetics: An Introduction,* Springer-Verlag, Berlin (1983).
12. H. A. Haus and E. P. Ippen, "Self-starting of passively mode-locked lasers," *Opt. Lett.* **16,** 1331–1333 (1991).
13. E. P. Ippen, L. Y. Liu, and H. A. Haus, "Self-starting condition for additive-pulse modelocked lasers," *Opt. Lett.* **15,** 183–185 (1990).
14. F. Krausz, T. Brabec, and C. Spielmann, "Self-starting passive mode-locking," *Opt. Lett.* **16,** 235–237 (1991).
15. J. Herrmann, "Starting dynamic, self-starting condition and mode-

locking threshold in passive, coupled-cavity or Kerr-lens mode-locked solid-state lasers," *Opt. Commun.* **98,** 111–116 (1993).
16. R. W. Boyd, *Nonlinear Optics,* Academic Press, New York (1992).
17. L. R. Brovelli, U. Keller, and T. H. Chiu, "Design and operation of antiresonant Fabry-Perot saturable semiconductor absorbers for mode-locked solid-state lasers," *J. Opt. Soc. Am. B* **12,** 311–322 (1995).
18. H. A. Haus, J. G. Fujimoto, and E. P. Ippen, "Structures for additive pulse modelocking," *J. Opt. Soc. Am. B* **8,** 2068–2076 (1991).
19. H. A. Haus, "Theory of modelocking with a fast saturable absorber," *J. Appl. Phys.* **46,** 3049–3058 (1975).
20. G. H. C. New, "Pulse evolution in mode-locked quasi-continuous lasers," *IEEE J. Quantum Electron.* **10,** 115–124 (1974).
21. J. D. Kafka, T. Baer, and D. W. Hall, "Mode-locked erbium-doped fiber laser with soliton pulse shaping," *Opt. Lett.* **14,** 1269–1271 (1989).
22. K. Smith, E. J. Greer, R. Wyatt, P. Wheatley, and N. J. Doran, "Totally integrated erbium fiber soliton laser pumped by laser diode," *Electron. Lett.* **27,** 244–245 (1990).
23. F. X. Kärtner, D. Kopf, and U. Keller, "Solitary pulse stabilization and shortening in actively mode-locked lasers," J. Opt. Soc. Am. B **12,** 486–496 (1995).
24. D. Kopf, F. Kärtner, K. J. Weingarten, and U. Keller, "Pulse shortening in a Nd:glass laser by gain reshaping and soliton formation," *Opt. Lett.* **19,** 2146–2148 (1994).
25. F. X. Kärtner and U. Keller, "Stabilization of soliton-like pulses with a slow saturable absorber," *Opt. Lett.* **20,** 16–18 (1995).
26. U. Keller, T. K. Woodward, D. L. Sivco, and A. Y. Cho, "Coupled-cavity resonant passive modelocked Nd:yttrium lithium fluoride laser," *Opt. Lett.* **16,** 390–392 (1991).
27. U. Keller and T. H. Chiu, "Resonant passive modelocked Nd:YLF laser," *IEEE J. Quantum Electron.* **28,** 1710–1721 (1992).
28. A. E. Siegman and D. J. Kuizenga, "Active mode-coupling phenomena in pulsed and continuous lasers," *Opto-electronics* **6,** 43–66 (1974).
29. G. P. Agrawal and N. A. Olsson, "Self-phase modulation and spectral broadening of optical pulses in semiconductor laser amplifiers," *IEEE J. Quantum Electron.* **25,** 2297–2306 (1989).
30. D. Kopf, K. J. Weingarten, L. Brovelli, M. Kamp, and U. Keller, "Diode-pumped 100-fs passively mode-locked Cr:LiSAF using an A-FPSA," *Opt. Lett.* **19,** 2143–2145 (1994).
31. N. H. Rizvi, P. M. W. French, and J. R. Taylor, "Generation of 33-fs pulses from a passively mode-locked Cr^{3+}:$LiSrAlF_6$ laser," *Opt. Lett.* **17,** 1605–1607 (1992).
32. G. P. A. Malcolm and A. I. Ferguson, "Self-mode locking of a diode-pumped Nd:YLF laser," *Opt. Lett.* **16,** 1967–1969 (1991).

Franz X. Kärtner studied electrical engineering at the Technical University Munich, where he received the Diploma degree in 1986 and the PhD degree in 1989. From 1991 to 1993 he was a Feodor-Lynen Research fellow of the Aleseander von Humboldt Foundation at Massachusetts Institute of Technology, USA. Since 1993 he has been with the Institute of Quantum Electronics, Swiss Federal Institute of Technology (ETH), Zurich, Switzerland. His research interests include noise in electronic circuits and optical devices, generation of squeezed states in the microwave and optical domain, quantum optics, and laser physics in general. His current research interest is focused on the dynamics of mode-locked lasers. Dr. Kärtner is a member of the German Physical Society and the Optical Society of America.

Luigi R. Brovelli received the Diploma degree in physics in 1988 and the PhD degree in natural sciences in 1993 from the Swiss Federal Institute of Technology in Zurich, Switzerland. From January 1989 to March 1993 he worked at the Laser Science and Technology Department of the IBM Zurich Research Laboratory on semiconductor lasers, especially strained-layer lasers, laser dynamics, and integrated mode-locked lasers. In April 1993 he joined the Institute of Quantum Electronics at the Swiss Federal Institute of Technology as a postdoctoral fellow. He is working on the design and characterization of novel semiconductor saturable absorbers for mode-locked solid state lasers.

Daniel Kopf studied physics at the Swiss Federal Institute of Technology (ETH), Zurich, Switzerland, where he received his diploma degree in 1992. Currently he is pursuing a PhD degree at the Institute of Quantum Electronics, ETH, Zurich. His current interest is focused on diode-pumped femtosecond lasers.

Markus Kamp studied physics at the Technical University of Aachen, Germany. After his Diploma (1989) he undertook research on growth and characterization of III-V semiconductors at KFA Jülich. Following his PhD (1992) he joined ETH Zurich as a postdoctoral research fellow. Here, he worked in close cooperation with IBM Research Lab. Zurich on semiconductor devices and lasers. Today he is with the Optoelectronics Department at the University of Ulm working on group III nitrides.

Irio Calasso studied physics at the Swiss Federal Institute of Technology (ETH), Zurich, Switzerland, where he received his diploma degree in 1994, working on the *Q*-switching dynamics of solid state lasers. Currently he is pursuing a PhD degree at the Institute of Quantum Electronics, ETH, Zurich. His current research interests are in infrared spectroscopy.

Ursula Keller received the Diploma in physics from the Federal Institute of Technology (ETH), Zurich, Switzerland, in 1984, and the MS and PhD degrees in applied physics from Stanford University, Stanford, California in 1987 and 1989, respectively. Her PhD research was on optical probing of charge and voltage in GaAs integrated circuits and on low-noise ultrafast laser systems. From late 1984 to 1985 she worked on optical bistability at Heriot-Watt University, Edinburgh, Scotland. In 1989, she joined AT&T Bell Laboratories, Holmdel, New Jersey, as a member of the technical staff, where she conducted research on photonic switching, ultrafast laser systems, and semiconductor spectroscopy. Since March 1993, she has been an associate professor in the Institute of Quantum Electronics at the Swiss Federal Institute of Technology (ETH) in Zurich, Switzerland. Her current research interests are in ultrafast lasers, semiconductor spectroscopy, and novel devices for applications in optical information processing, communication, and medicine. Professor Keller is a member of the Optical Society of America and the Institute of Electrical and Electronics Engineers. During 1985–1986 she was a Fulbright Fellow, and in 1987–1988 she received an IBM Predoctoral Fellowship.